TB, RML, US, PhysBio/364692, 18/02/2011

IOP PUBLISHING PHYSICAL BIOLOGY

Phys. Biol. **8** (2011) 000000 (9pp) UNCORRECTED PROOF

Quantification of nanoscale density fluctuations by electron microscopy: probing cellular alterations in early carcinogenesis*

Prabhakar Pradhan[1,5], Dhwanil Damania[1], Hrushikesh M Joshi[2], Vladimir Turzhitsky[1], Hariharan Subramanian[1], Hemant K Roy[3], Allen Taflove[4], Vinayak Dravid[2] and Vadim Backman[1]

[1] Biomedical Engineering Department, Northwestern University, Evanston, IL 60208, USA
[2] Department of Material Science and Engineering, Northwestern University, Evanston, IL 60208, USA
[3] Department of Internal Medicine, NorthShore University HealthSystem, Evanston, IL 60208, USA
[4] Department of Electrical Engineering and Computer Science, Northwestern University, Evanston, IL 60208, USA

E-mail: pradhan@northwestern.edu

Received 1 August 2010
Accepted for publication 13 January 2011
Published DD MMM 2011
Online at stacks.iop.org/PhysBio/8/000000

Abstract

Most cancers are curable if they are diagnosed and treated at an early stage. Recent studies suggest that nanoarchitectural changes occur within cells during early carcinogenesis and that such changes precede microscopically evident tissue alterations. It follows that the ability to comprehensively interrogate cell nanoarchitecture (e.g., macromolecular complexes, DNA, RNA, proteins and lipid membranes) could be critical to the diagnosis of early carcinogenesis. We present a study of the nanoscale mass-density fluctuations of biological tissues by quantifying their degree of disorder at the nanoscale. Transmission electron microscopy images of human tissues are used to construct corresponding effective disordered optical lattices. The properties of nanoscale disorder are then studied by statistical analysis of the inverse participation ratio (IPR) of the spatially localized eigenfunctions of these optical lattices at the nanoscale. Our results show an increase in the disorder of human colonic epithelial cells in subjects harboring early stages of colon neoplasia. Furthermore, our findings strongly suggest that increased nanoscale disorder correlates with the degree of tumorigenicity. Therefore, the IPR technique provides a practicable tool for the detection of nanoarchitectural alterations in the earliest stages of carcinogenesis. Potential applications of the technique for early cancer screening and detection are also discussed.

1. Introduction

Cancer is one of the leading causes of death in the United States and worldwide [1]. Cell morphology, from molecular to cellular levels, is inherently linked to biochemical, biomechanical and transport processes within the cell. Examples include the effects of high-order chromatin structure on gene transcription and genetic information flow in the nucleus [2–5], macromolecular crowding on the cytoskeleton, biomechanical properties and protein folding in the cytoplasm [6–8]. Although a significant body of knowledge regarding genetic and epigenetic alterations in carcinogenesis has been accumulated, structural intracellular changes and their role in carcinogenesis are still incompletely understood. Conventional visible-light microscopy techniques

* Originally submitted for the physical oncology special focus issue.

[5] Author to whom any correspondence should be addressed.

allow detection of morphological changes at the micron and supramicron scales in tissues/cells that are prominent in the later stages of carcinogenesis (i.e. dysplasia) resulting from multiple genetic and epigenetic alterations [9–12]. However, understanding the earlier initiating morphological events in carcinogenesis requires the ability to detect nanoarchitectural changes, which, at best, remains challenging. In particular, the ability to comprehensively interrogate the nanoarchitecture of cells and tissues is critical for applications that require an understanding of the role of cell nanoarchitecture in early carcinogenesis [5, 13]. To date, the nanoarchitectural properties of cells/tissues have not been well understood or studied.

As suggested by several recent studies, the progression of cancer in the early stages is accompanied by nanoscale morphological or architectural changes in the internal cell structure that precede histological abnormalities. Such changes result in nanoscale mass-density fluctuations in cells. While conventional visible-light microscopy techniques have been widely used to characterize biological systems, their ability to detect changes at the nanoscale is fundamentally impeded by their diffraction-limited resolution [14]. However, recent spectral optical microscopy studies have shown that such nanoscale fluctuations manifest themselves prominently in early carcinogenesis [15–17]. Furthermore, these studies indicate that changes in nanomorphology occur at length scales of approximately 10–100 nm, which reflect the length scale associated with the cellular building blocks (e.g., DNA, RNA, proteins and lipids). However, far-field optical techniques are unable to probe the detailed nature of these nanoscale changes. This obstacle led us to explore the potential of transmission electron microscopy (TEM) with its nanoscale (∼1 nm) resolution. TEM imaging techniques have been widely used to visualize nano- and micro-structures in biological samples [18]. Still, the quantitative information embedded within a TEM image in the context of biological sub-structure is poorly understood, in particular, subtle short-range nanoscale fluctuations and correlations of the grayscale, as well as the changes of such fluctuations with the pathogenesis of disease states [19].

To quantify the mass-density fluctuations, we utilized an idea from condensed-matter physics and applied it to biological systems. This concept involves construction of optical lattices from the mass-density fluctuations derived from TEM images of cells/tissues, and then statistically analyzing the localization characteristics of the eigenfunctions of these disordered lattices via the average value of the inverse participation ratio (IPR) of these eigenfunctions. The IPR of an eigenfunction E is defined as

$$\mathrm{IPR} = \int |E(r)|^4 \, \mathrm{d}\vec{r} \tag{1}$$

(in units of inverse area in two dimensions). The optical-localization properties of these lattices are directly related to the statistical average value of the IPR. The statistical properties of IPR are important quantitative measures of the spatial localization of the eigenfunctions in optical lattices (i.e. either ordered or disordered). In two-dimensional (2D) optical lattices, (i) the average value of IPR for a uniform lattice is a fixed universal number (approximately 2.5 in the unit of the inverse area) and (ii) the average IPR value increases from a uniform lattice to a disordered lattice with an increase in the degree of the disorder. Moreover, in 2D, the value of IPR not only depends on the mass-density fluctuations, but also the correlation length of these fluctuations (Lc). The average value of the IPR is proportional to the refractive index fluctuation (Δn) of optical media and corresponding fluctuation correlation decay length (Lc), or $\langle IPR \rangle \alpha \Delta n \times Lc$. This has been well studied in condensed-matter physics for characterizing the disorder properties of localization and the quantum Hall effect [20–23].

In a recent short letter [24] we showed that applying the IPR technique we could measure and differentiate the degree of disorder at the nanoscales in microscopically similar cells, but with different malignant potential. In particular, we used human colon cancer cell line HT29 and its genetic variant to study the degree of disorder via IPR analysis of their TEM images. The IPR technique was enabled to quantify the degree of disorder at the nanoscale and their relative variation in otherwise microscopically similar cells with different malignant potential for human colon cancer cell line HT29 and its genetic variance (CSK). In this study, we also validated the IPR technique of TEM image analysis by using model disordered nanoparticle systems, that is, using nano-disordered dielectric samples of known parameters. Furthermore, rigorous numerical simulations were performed for cell like weakly disordered media to establish the relation between IPR and the disorder parameters of the samples to confirm $\langle IPR \rangle \alpha \Delta n \times Lc$. In the context of the biological study, the significance of this relation is related to the degree of disorder which is related to the morphological condition in a cell in carcinogenesis. Specifically, $\langle \mathrm{IPR} \rangle$ provides the measure of the degree of disorder of refractive index fluctuations in biological media due to light scattering in this closed media.

In this paper, we first discuss the methodology for quantifying nanoscale mass-density fluctuations in detail. A short description was presented in [24] about the methodology, but here we present the methodology in detail (section 2). Then we review in brief our previous results [24] to provide a background for the present study (section 3). Finally, for the first time, we report the results of the quantification of the nanoscale mass-density fluctuations in human colon tissues and their alterations in early carcinogenesis (section 4.1). We further study the correlation between the nanoscale fluctuations and tumorigenicity (or the degree of malignancy) in colon early carcinogenesis (section 4.2). We conclude the results and discuss the potential application of the technique for early cancer detection and screening at the end (section 5).

2. Inverse participation ratio analysis technique for biological cells/tissues

2.1. Construction of optical lattices

A short description of the methodology was presented in [24], but here we present the methodology in detail. The

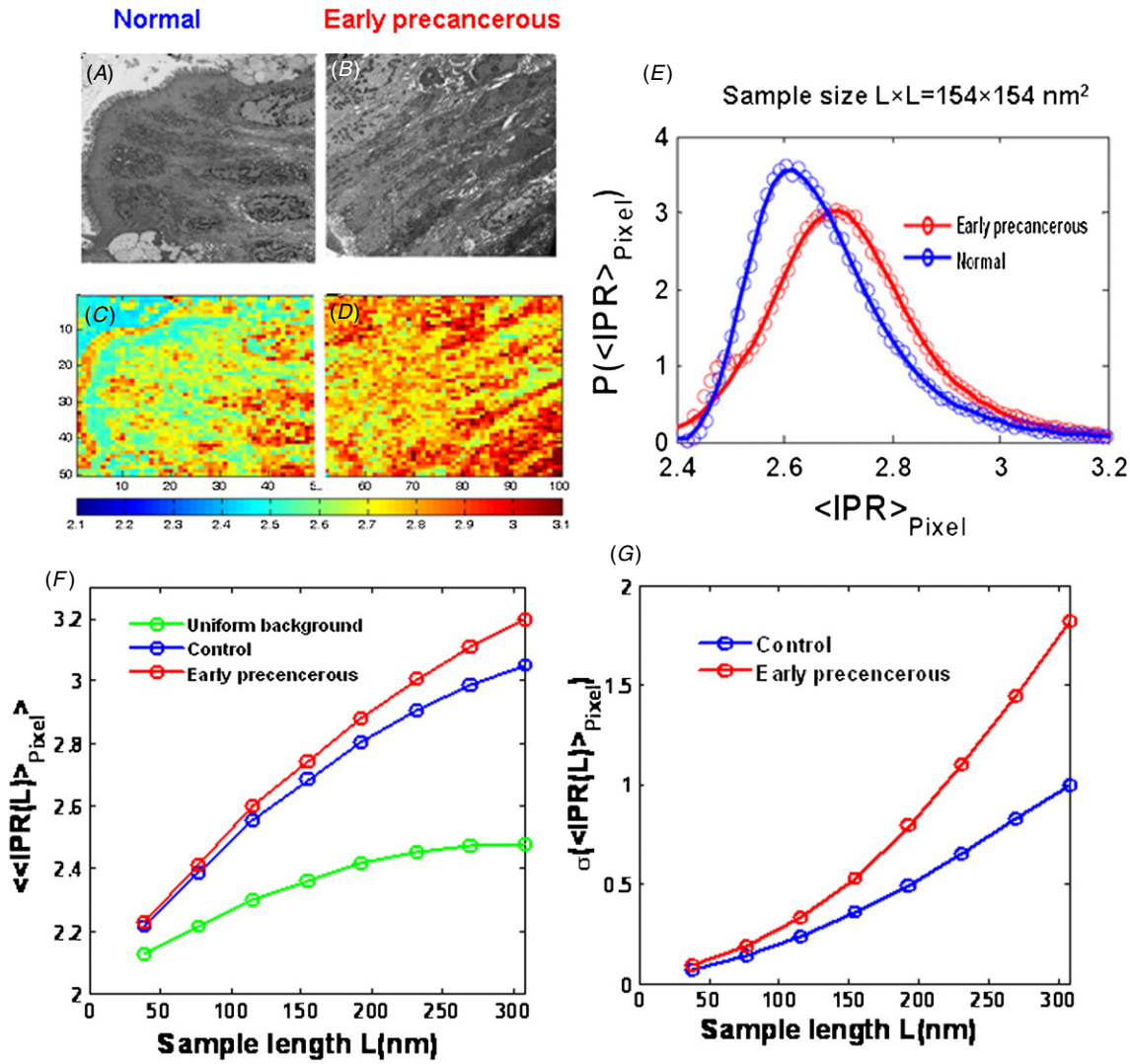

Figure 1. (*A*) and (*B*) Representative TEM images of tissues from normal patients and patients harboring colonic adenometous polyps. (*C*) and (*D*) Corresponding IPR-pixel images for the pixel size 154 nm × 154 nm (unit grid length is 7.7 nm). (*E*) Relative $\langle \mathrm{IPR}(L)\rangle_{\mathrm{Pixel}}$ distributions (ensemble) of IPR-pixel sizes $L \times L = 154$ nm × 154 nm for rectal tissues from normal patients and early precancerous patients. (*F*) Ensemble-averaged values of the IPR-pixel $\langle\langle \mathrm{IPR}(L)\rangle_{\mathrm{Pixel}}\rangle$ versus L (in nm) plots for (i) uniform background, (ii) normal tissues and (iii) early precancerous tissues. (*G*) Corresponding standard deviation $\sigma(\langle \mathrm{IPR}(L)\rangle_{\mathrm{Pixel}})$ versus L (in nm) plots for normal tissues and early precancerous tissues. (Because of the large number of samples, error bars are negligible in (*F*) and (*G*).)

TEM grayscale intensity, I_{TEM}, decays exponentially with the thickness of the sample, where the decay constant is a function of the mass density [9]. This exponential decay can be approximated as a linear decay for a very thin sample, when the sample length is much smaller than the decay length scale. TEM studies of thin layers of nanoscale dielectric beads have shown that I_{TEM} is linearly proportional to the mass density of the beads [25, 26]. For a very thin biological sample, one can assume that the grayscale TEM image intensity at any lattice point around the point (x, y), $I_{\mathrm{TEM}}(x, y)$ (see figures 1*(A)–(D)*), is linearly proportional to the total scattering strength and, hence, the mass $M(x, y)$ (total biomass of the biological samples) present in the corresponding tissue voxel around the lattice point (dimensions: 10 nm × 10 nm in the x–y plane; 70 nm along the z-direction) of the sample slices. In this paper, all the TEM studies are related to the biological samples of thin films, therefore we will consider them as 2D samples.

It has been well studied and shown that the optical refractive index (n) is linearly proportional to the local density (ρ) of intracellular macromolecules, such as proteins, lipids, DNA and RNA, i.e.$n = n_0 + \Delta n = n_0 + \alpha\rho$, where n_0 is the refractive index of the medium surrounding a scattering structure, ρ is the local concentration of solids, and α is a proportionality constant. The studies further showed that the majority of the scattering substances found in living cells have approximately the same value of the proportionality constant $\alpha \sim 0.18$ [27, 28]. Furthermore, we consider that the absorption of the contrast agent by the biomass of the thin tissue voxel is linearly proportional to the total mass present in the voxel and that the lattice is an effective optical lattice. We consider that the refractive index at the voxel around the point (x, y) is $n(x, y)$. Therefore $n(x, y)$ is functionally proportional to its biomass and we can write

$$n(x, y) = f(M(x, y)) = f(I_{\mathrm{TEM}}(x, y)). \qquad (2)$$

We further assume that the form of I_{TEM} at (x, y) is given by

$$I_{\mathrm{TEM}}(x, y) = I_0 + \Delta I_{\mathrm{TEM}}(x, y), \tag{3}$$

where I_0 is the mean background of the whole TEM sample, and $\Delta I_{\mathrm{TEM}}(x, y)$ is the fluctuating part of the intensity around a spatial point (x, y) of the pixel. Then, the refractive index of a tissue voxel from the corresponding TEM pixel can be written as

$$\begin{aligned} n(x, y) &= n_0 + \Delta n(x, y) = f(I_{\mathrm{TEM}}(x)) \\ &= f_0 + f_0' \times \Delta I_{\mathrm{TEM}}(x, y), \end{aligned} \tag{4}$$

where n_0 is the constant-background part of the full sample, and $\Delta n(x, y)$ is the fluctuating part of the refractive index $n(x, y)$. It can be shown that the effective optical potential of an optical lattice, ε_i, has the following form [29, 30]:

$$\varepsilon_i \propto \Delta n(x, y)/n_0 = (\Delta I_{\mathrm{TEM}}(x, y)/I_0) \times (I_0 \times f_0'/f_0), \tag{5}$$

where fluctuating TEM intensity $\Delta I_{\mathrm{TEM}}(x, y) \ll I_0$ and $\Delta n(x, y) \ll n_0$. This is a good approximation, this is because for tissue the range of $n_0 = 1.33$–1.38 and the range of $\Delta n = 0.01$–0.1. The exact eigenfunctions $(E_i(x, y), i = 1{-}N)$ of each two-dimensional pixel of optical sample size of area $L \times L$ can be calculated by solving the wave equation for the electric field in the lattice using a disorder tight-binding model [29, 30].

2.2. Tight-binding model and IPR statistics

To quantify the disorder properties of the TEM images, we have carried out numerical calculations of the Anderson disorder tight-binding model (TBM). The TBM has been well studied, and it has proven to be a good model for describing single-optical states or localized optical states of systems of any geometry and disorder. In our study, we consider one optical state of a photon per lattice site, and the interlattice site hoppings are restricted to the nearest neighbors only. Such a Hamiltonian can be written as [29, 30]

$$H = \sum_i \varepsilon_i |i\rangle\langle i| + t \sum_{\langle ij \rangle} |i\rangle\langle j| + |j\rangle\langle i|, \tag{6}$$

where $\varepsilon_i \propto \Delta n(x, y)/n_0$ is the ith lattice site energy; $|i\rangle$ and $|j\rangle$ are the optical eigenfunctions at the ith and jth lattice sites, respectively; $\langle i\, j\rangle$ indicates the nearest neighbors; and t is the overlap integral between sites i and j.

In our analyses, for short-length refractive index fluctuations, a large TEM micrograph (in our study 15.8 μm × 15.8 μm as shown in figures 3(A) and (B) is virtually cut into smaller ((77 nm × 77 nm)–(308 nm × 308 nm)) samples or IPR pixels. To project the TEM image to the tight-binding model, the fluctuating part of every grayscale point of the TEM image is first considered proportional to the onsite optical potential energy ε_i (i.e. using equation (5)). The optical potential is obtained by first projecting the optical wave equation to the Schrödinger equation, and then equating the optical potential of the optical wave equation with the potential of the Schrödinger equation. Finally, in the tight-binding model, the optical potential ε_i is then rescaled such that its mean is the same as the hopping parameter, i.e. $t = \mathrm{mean}(\varepsilon_i)$, and we further consider $(I_0(x, y) f_0'/f_0)/t = \text{constant} = 1$, without any loss of generality.

The average value of the IPR of a pixel of side length L, $\langle \mathrm{IPR} \rangle_{\mathrm{Pixel}}$, (area $L \times L$) can then be written as [20–22]

$$\langle \mathrm{IPR}(L) \rangle_{\mathrm{Pixel}} = \frac{1}{N} \sum_{i=1}^{N} \int_0^L \int_0^L E_i^4(x, y)\, \mathrm{d}x\, \mathrm{d}y, \tag{7}$$

where E_i is the ith eigenfunction of the Hamiltonian in equation (6) of an optical lattice (i.e. an IPR pixel) of size $L \times L$; $N = L_a^2$ ($L_a = L/a$ (lattice size), $a = \mathrm{d}x = \mathrm{d}y$) is the total number of the eigenfunctions; and $\langle\ \rangle_{\mathrm{Pixel}}$ denotes the average over all the N eigenfunctions of the IPR pixel. Importantly, this derivation process mainly considers the fluctuating part of n relative to its average background as the rescaled potential. The statistical analyses of the IPR were done by taking the ensemble averaging and std of the samples of a fixed size over biological tissues from a single patient and then averaging from several patients.

3. Previous studies using the IPR analysis

In this section we briefly review our previous results reported in [24] to provide a background of the present study of the precancerous tissues. In the study, it was shown that the IPR technique can be used to quantify minute changes in nanoscale disordered dielectric (optical) media comprising a known, controlled disordered model system. Then we showed that the IPR technique can be used to differentiate between two types of cell lines with different malignancy.

3.1. Validation of the IPR technique using nano-disordered media

In order to investigate the hypothesis that IPR technique can accurately quantify nanoscale disorder changes, we performed TEM studies on model experimental systems of dielectric nanoparticles (average diameter ∼6 nm, standard deviation ∼2 nm) [24]. Dielectric nanoparticles, which act as disordered scatterers in a concentration-dependent manner, were deposited on a formvar thin dielectric film. The goal of this study was to determine whether the short-length-scale disorder strength could be measured by the IPR technique and how the average value of IPR changes with an increase in the nanoparticle density or the scattering mean-free path. Given the ultrafine size of the nanoparticles used in these experiments and their random orientation and spatial distribution, the TEM image contrast is dominated by mass thickness, with minimal average contribution from diffraction and phase contrast under the imaging conditions employed. While much simpler than a biological system, this model allowed us to control and characterize the disorder strength. Both, the model and biological systems, have an average uniform refractive index background (n_0) and weaker refractive index fluctuations (Δn) above the uniform background ($\Delta n/n_0 \ll 1$).

For the main result, we performed length scale dependent of $\langle \langle \mathrm{IPR}(L) \rangle_{\mathrm{Pixel}} \rangle$. The result showed that $\langle \langle \mathrm{IPR}(L) \rangle_{\mathrm{Pixel}} \rangle$

value is proportional to the product of the amplitude of the refractive index fluctuation and its correlation. Overall, the validation study in [24] showed that the nanoscale disorder can be quantified by the IPR technique, which can distinguish statistically significant differences between the two disordered systems of minute difference in disorder.

3.2. IPR study of cell lines: nanoscale mass-density fluctuation analysis of HT29 cells and their CSK-knockdown genetic variant

To investigate the changes in nanoscale mass-density fluctuations with the progression of carcinogenesis, we performed experiments on the well-characterized HT29 colon cancer cell line and its CSK-knockdown genetic variant, which was engineered via knockdown of the tumor suppressor gene c-terminus src kinase, leading to more aggressive neoplastic behavior of these cells [24]. The increase of the nanoscale disorder (in particular, increase of the disorder strength parameter $L_d = \Delta n^2 \times Lc$) with the progression of carcinogenesis was shown in our prior optical experiments using partial wave spectroscopic microscopy (PWS) for the same cell line study [15–17]. HT29 cells, which were used as a control in the experiment, were actually a human colonic adenocarcinoma cells that were able to express differentiation features which are characteristic of mature colonic cells. The knockdown of the tumor-suppressor *CSK*, a gene which is knocked down in most colon cancers, increases the growth/proliferation of HT29 cells. In TEM experiments on these cells, we were interested to observe the effect of carcinogenesis in terms of intracellular mass-density fluctuations at the nanoscale. We noted that all cells used for the experiment were otherwise cytologically (i.e. microscopically) indistinguishable.

The length scale-dependent analyses of the average and std of IPR with the increasing sample length for the HT29 and CSK cells were studied. Our results showed that the average $\langle\langle \mathrm{IPR}(L)\rangle_{\mathrm{Pixel}}\rangle$ and the std $\sigma(\langle \mathrm{IPR}(L)\rangle_{\mathrm{Pixel}})$ values are higher for the more malignant CKS cells relative to the less malignant HT29 cells, *with a significant p-vale (<.05)*. Both $\langle\langle \mathrm{IPR}(L)\rangle_{\mathrm{Pixel}}\rangle$ and $\sigma(\langle \mathrm{IPR}(L)\rangle_{\mathrm{Pixel}})$ increased with increasing L for the CSK cells relative to the HT29 cells, indicating a relatively greater degree of disorder or nanoscale fluctuations for the CSK cells, relative to HT29 cells.

The above results of the cell line study motivate us to study the nanoscale fluctuations in precancerous human tissues for early cancer detection using IPR technique.

4. Results of the human precancerous colonic tissue study

4.1. Nanoscale mass-density fluctuation of normal and early precancerous colon tissues

To investigate the hypothesis that nanoscale mass-density fluctuations increase with the progression of carcinogenesis, we performed experiments on colonic tissues from control and precancerous patients. Based on the results reviewed in the previous section, in this paper, we investigate whether the IPR technique is applicable in measuring the early signatures of nanoscale mass density changes in tissues via the 'field-effect' phenomenon. Many early cancer screening techniques are designed to exploit the 'field effect' of carcinogenesis. The 'field effect' is a proposition that the genetic/environmental milieu that results in neoplasia in one region of an organ should be detectable throughout the organ [17, 31, 32]. In particular, we wanted to test this 'field effect' model for colon carcinogenesis by measuring the nanoarchitectural changes in rectal cells/tissues of patients who have premalignant adenomatous polyps in their colon.

4.1.1. Tissue sample collection. To this end, we carried out a pilot study involving IPR analyses of 10 human subjects. Biopsies from endoscopically normal rectal mucosa were acquired from these subjects at the time of their colonoscopies in accordance with standard clinical practice. The colonoscopies indicated that five subjects harbored precancerous adenomatous polyps (the size of adenomatous polyps ranged from 2 to 10 mm) in their colon, while the other five subjects were free from adenomas. All tissue samples appeared histopathologically normal. TEM images were then acquired following the same protocol as described below.

4.1.2. Sample preparation for TEM and TEM imaging. The biopsy samples were first placed in Karnovsky's fixative for 2 weeks to preserve structure. The fixative consists of 0.1 M phosphate buffered solution containing 5% glutaraldehyde with pH between 7.2 and 7.4. Following a standard protocol, the samples were stained with osmium tetraoxide (OsO_4), dehydrated, and then embedded in resin containing 36% ERL 4221, 12% diglycidyl ether of polypropyleneglycol (DER 736), 51% nonenyl succinic anhydride (NSA), and ∼1% dimethylaminoethanol (DMAE) by mass. Samples were then sectioned with an ultra-microtome to a thickness of 70 nm.

4.1.3. TEM imaging. Finally, TEM micrographs were obtained (JEM-1400, JEOL, Tokyo, Japan) for each of the prepared samples from different patients (control and precancerous). A 200 keV electron beam with a fixed magnification (40 K) was used for each micrograph.

4.1.4. Statistical analysis. For the statistical analysis, we took tissue samples from $n = 5$ control patients and $n = 5$ precancerous patients. We collected ∼15–20 separate tissue samples from the different parts of the rectum of each patient, and TEM micrographs were prepared for each tissue sample. We randomly chose 10 TEM micrographs of independent tissue samples for each patient. In particular, an ensemble of 50 independent TEM micrographs of independent tissues (i.e. 50 independent measurements) from control patients ($n = 5$, 10 micrographs per patient) and 50 independent micrographs (i.e. 50 independent measurements) of early precancerous patients ($n = 5$, 10 micrographs per patient) were taken for the statistical significance of the IPR difference study.

Figures 1(*A*) and (*B*) show representative TEM grayscale images of rectal tissue samples from adenoma-free subjects and from subjects harboring precancerous adenomatous polyps in their colon. Figures 1(*C*) and (*D*) show the corresponding IPR images (IPR pixel dimension = 154 nm × 154 nm). The IPR images clearly indicate different disorder states for tissues obtained from the normal and the early precancerous subjects.

Figure 1(*E*) shows the distribution $P(\langle \mathrm{IPR}(L)\rangle_{\mathrm{Pixel}})$ for rectal tissues from the normal and the early precancerous subjects for IPR pixel sizes $L \times L = 154$ nm $\times 154$ nm. This shows a distinct separation between the two groups of subjects.

Figure 1(*F*) shows plots of $\langle\langle \mathrm{IPR}(L)\rangle_{\mathrm{Pixel}}\rangle$ versus L for three different cases: (i) uniform lattice, (ii) rectal tissues from the normal subjects, and (iii) rectal tissues from the early precancerous subjects. Here, $< >$ denotes the ensemble averaging (averaged over ∼500 000 IPR pixels for the sample size $L \times L = 77$ nm × 77 nm and averaged over ∼125 000 IPR pixels for the sample size $L \times L = 154$ nm × 154 nm). Figure 1(*G*) shows plots of the corresponding standard deviation $\sigma(\langle \mathrm{IPR}(L)\rangle_{\mathrm{Pixel}})$ versus L.

The three curves in figure 1(*F*) clearly show that the $\langle\langle \mathrm{IPR}(L)\rangle_{\mathrm{Pixel}}\rangle$ value is highest for rectal tissues from the early precancerous subjects. For example, $\langle\langle \mathrm{IPR}(L)\rangle_{\mathrm{Pixel}}\rangle$ values for the uniform background, the normal-subject rectal tissues, and the early precancerous-subject rectal tissues are 2.5, 3.053 and 3.196, respectively. Student's *t*-test, two-tailed unequal variance *p*-value = 0.021, which is *statistically significant.*

Higher values of the average IPR correspond to larger disorder strengths by increased nanoscale fluctuations in the tissues. Importantly, figure 1(*F*) also shows that the ratio $\sigma(\langle \mathrm{IPR}(L)\rangle_{\mathrm{Pixel}})/\langle\langle \mathrm{IPR}(L)\rangle_{\mathrm{Pixel}}\rangle$ increases much faster with increasing L for the early precancerous-subject rectal tissues relative to the normal-subject rectal tissues. The rapid increase of this ratio is attributed to the long tails in the IPR distributions.

Figure 1 provides substantial evidence that microscopically normal-appearing colonic epithelial cells in early carcinogenesis exhibit a higher degree of nanoscale disorder than the cells from a control patient. These results suggest that IPR has the potential to detect early carcinogenic alterations in the human colon.

Importantly, the data given in figures 1 (*F*) and (*G*) show that the difference in average and standard deviation of IPR between control and adenoma patients appears to be around L ∼ 75 nm, but more prominent around L ∼ 100 nm. This is the building block of the cell/tissue (DNA, RNA, Lipids, proteins, etc).

Further, we have calculated the intratissue/intramicrograph correlation for $\langle \mathrm{IPR}\rangle_{\mathrm{Pixel}}$, which shows ∼0.148 as the correlation coefficient (50 micrographs of independent tissues from control patients and 50 micrographs of independent tissues from five adenoma patients for a total of 100 independent tissue micrographs). Furthermore, we have calculated the intrapatient correlation for $\langle \mathrm{IPR}\rangle_{\mathrm{Pixel}}$, showing that the correlation coefficient is ∼0.031 (for five control patients and five adenoma patients). These results indicate that the average nanoscale fluctuations within a cell, in part of a cell, or in a patient are quite randomly distributed, i.e. having weaker correlations.

4.2. Nanoscale mass-density fluctuation and tumorigenicity correlation

In this section we study the correlation of nanoscale mass-density fluctuations with tumorigenicity. In particular, to quantify the correlation between the degrees of developing malignant phenotype (i.e. tumorigenicity) and increase in the degree of nanoscale mass-density fluctuations (i.e. the average IPR value), we further studied the relative IPR values for the above five adenoma patients according to their clinically classified tumorigenicity. Most colon cancers progress through a precursor lesion, the premalignant adenomatous polyp [33]. The degree of tumorigenicity of colonic adenomas (i.e. the risk of progression into cancer) depends on their size and histology and increases from diminutive adenomas (polyps size < 5 mm) to 5–9 mm adenomas to advanced adenomas (polyp size ⩾10 mm, high-grade dysplasia or ⩾25% villous features) [34, 35]. Accordingly, in our study, the patients with adenomas were divided into three categories: patients with diminutive adenoma ($n = 2$ patients), patients with non-diminutive, non-advanced adenoma ($n = 2$) and patients with advanced adenoma ($n = 1$). Given that IPR increase parallels the degree of malignant aggressiveness of cell lines, we hypothesized that IPR would not only be increased in the field of carcinogenesis (patients harboring adenomas), but that its value would also correlate with the malignant potential of these premalignant lesions.

In figure 2 we plotted the average IPR for patients without adenomas and patients harboring adenomas of progressively increasing tumorigenicity. Each average $\langle\langle \mathrm{IPR}\rangle\rangle$ value was calculated over ∼50 000 IPR pixels, with sample size 154 nm × 154 nm. The figure clearly indicates an increasing trend in the average IPR value, and the data show that such trend correlates well with the increase of tumorigenicity. The same trends were obtained for other IPR pixel sizes (i.e. for any pixel size 30 nm×30 nm to 308 nm×308 nm). These results underscore the potential of using the IPR technique and the average IPR value obtained as a biomarker of colorectal carcinogenesis at the early stages [35].

We further calculated the statistical significance of the difference in the average IPR values over the tissue micrographs of control ($n = 5$, 50 independent tissue measurements/micrographs) and the IPR values of the three different adenoma sub-categories: diminutive adenoma ($n = 2$, 30 different tissue micrographs), non-diminutive adenoma ($n = 2$, 30 different tissue micrographs) and advanced adenoma ($n = 1$, 20 different tissue micrographs). Student's *t*-test, two-tailed unequal variance *p*-values are as follows: (i) between control and diminutive adenoma patients, *p*-value = 0.67 (which is consistent with published results reported in [34, 35]. (b) Between control and non–diminutive adenoma, *p*-value = 0.03. (c) Between control and advanced adenoma, *p*-value = 0.05. Overall, the results show a correlation between

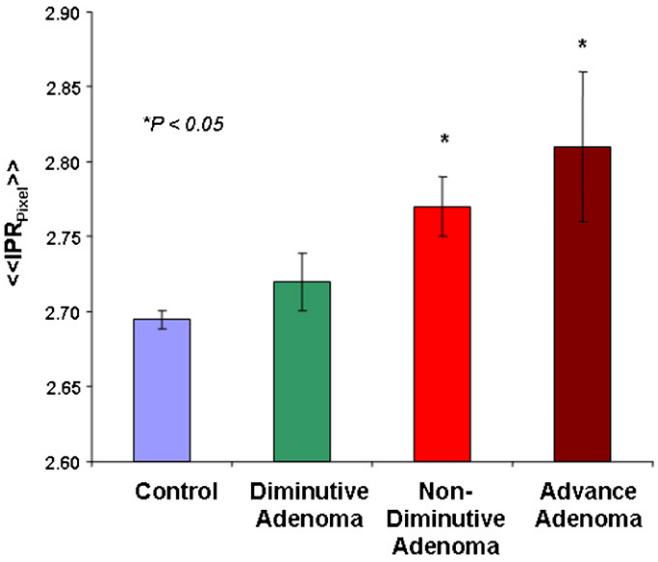

Figure 2. Average IPR value versus tumorigenicity plot. $\langle\langle \mathrm{IPR}(L)\rangle_{\mathrm{Pixel}}\rangle$ values are plotted with the degree of tumorigenicity (pixel size $L \times L = 154$ nm $\times$ 154 nm and ensemble averaging both performed over ~50 000 pixels) for (i) control, (ii) diminutive adenoma, (iii) non-diminutive adenoma and (iv) advanced adenoma. There is an elevation of the IPR value with the degree of tumorigenicity, which shows a correlation between the degree of disorder and tumorigenicity.

tumorigenicity and an increasing trend of the average IPR value.

5. Discussion and summary

We have presented an IPR analysis technique to quantify the short-range nanoscale degree of disorder associated with nanoscale mass-density fluctuations of biological cells and tissues as inferred from scattered intensity in TEM. These can also be interpreted as the spatial localization properties of the optical eigenfunctions of the nanoscale optical disordered lattices of these cells and tissues. Our IPR analysis technique is unique in that it enables us to quantify the disorder in a single parameter (average *IPR* value ($\sim \Delta n \times Lc$)) that takes into account spatial/structural disorder and heterogeneous properties of the media. Our results show that the IPR technique can distinguish between tissues from control patients and precancerous patients. Given sole mass-thickness contrast and absence of any diffraction or phase contrast in TEM, we assumed (1) a mean absorption coefficient of the tissue biomass for the TEM contrast agent and (2) linearity between TEM grayscale image fluctuations and the effective refractive-index fluctuations. These two assumptions are plausible for thin samples and for weak mass-density fluctuations.

We briefly reviewed our previous results which show that the IPR technique enables us to quantify minute changes in nanoscale disordered dielectric (optical) media comprising a controlled disordered model system. This indicates that the IPR is an important parameter for quantifying nanoscale disorder. Next, we reviewed briefly IPR analysis to a controlled experimental study involving human colon cancer cells: the HT29 cell line and its more aggressive (but otherwise cytologically indistinguishable) CSK-knockdown genetic variant. It was found that the IPR technique reveals CSK-knockdown cells as having significantly larger nanoscale mass-density fluctuations than HT29 cells [24].

Finally, we found experimental evidence derived from human subjects, for increased disorder of nanoscale refractive-index fluctuations (i.e. increased average IPR values) associated with otherwise histologically normal mucosa in colon field carcinogenesis. Furthermore, the results of this pilot study indicate that the increase in the IPR (i.e. increase in nanoscale mass-density fluctuations) is correlated with a corresponding increase in *tumorigenicity* (i.e. the increase in lifetime risk of developing colorectal cancer). This evidence suggests that the IPR technique is the first approach that enables quantifying/imaging the field effect of colon carcinogenesis [16] using electron microscopy images. Until now, quantification of morphological alterations in the earliest stage of carcinogenesis has not been reported using electron microscopy image analysis. Only molecular (e.g., genetic, epigenetic and proteomics) alterations have been described. The increase in the nanoscale disorder reported here using the IPR technique may represent the earliest morphological alteration in carcinogenesis known to date.

For these colonic tissues, the results also show that the visible nanoscale changes occur around the length scale ~100 nm, which is on the order of the building blocks of the cells, including, for example, lipids, proteins, DNA and RNA. Importantly, the cell study showed similar results [24]. This indicates the possibility of nanoscale rearrangements in a cell/tissue at the building blocks level in early carcinogenesis.

We hypothesize that there could be several potential independent or correlated biological mechanisms which can alter the cell nanoarchitecture in early carcinogenesis that can be detected by IPR analysis. For example, the increase in IPR within a nucleus can be attributed to the chromatin compaction in it [36], leading to an increase in nanoscale mass-density fluctuations in more aggressive cells. In the case of HT29 and CSK cells, there appears to be a difference in the nanoscale cytoskeletal organization in both nucleus and cytoplasm [37] which may partially contribute to the increase in the average IPR value between HT29 control cells and CSK constructs. Similarly, there are reports suggesting defective cytoskeleton organization in the cultured fibroblasts of patients with inherited adenocarcinoma in colon and rectum [38]. The gradient increase in the average IPR value from control patients to those harboring different types of adenomas can be partly correlated to the changes in the cytoskeletal organization in the colon tissue of these individuals. Since IPR depends on the mass-density fluctuations and correlation length of these fluctuations (Lc), higher differential average IPR value implies increase in Lc which can be correlated to the increase in fractal dimension of the sub-cellular structures within the tissue as reported. [39, 40]

We anticipate that IPR analyses of TEM, as well as scanning transmission electron microscopy (STEM) images, will have potential applications for tissue/cell characterizations in basic biological research, as well as medical applications in detecting early-stage cancers. This also demands a larger population of patients, a study which is currently underway.

Acknowledgments

This work was supported by NIH grants (nos R01EB003682, R01CA128641 and U54CA143869) and NSF grant no CBET-0937987. VPD acknowledges support from NIH/NCI PS-OC grant no DMR-0603184 and NIH-CCNE (Northwestern) grant no U54CA119341. Parts of the experiments were done at the EPIC/NIFTI facility of the NU*ANCE* Centre (supported by NSF NSEC, NSFMRSEC, Keck Foundation, the State of Illinois, and Northwestern University) at Northwestern University. PP thanks S Sridhar (Northeastern University, Boston) for many encouraging and insightful discussions.

Q3 ## References

[1] Jemal A *et al* 2009 Cancer Statistics, 2009 *CA Cancer J. Clin.* **59** 225–49
[2] Delcuve G P, Rastegar M and Davie J R 2009 Epigenetic control *J. Cell. Physiol.* **219** 243–50
[3] Mohn F and Schubeler D 2009 Genetics and epigenetics: stability and plasticity during cellular differentiation *Trends Genet.* **25** 129–36
[4] Adams P D 2007 Remodeling of chromatin structure in senescent cells and its potential impact on tumor suppression and aging *Gene* **397** 84–93
[5] Zuckerkandl E and Cavalli G 2007 Combinatorial epigenetics, 'junk DNA', and the evolution of complex organisms *Gene* **390** 232–42
[6] Lawlis S J, Keezer S M, Wu J R and Gilbert D M 1996 Chromosome architecture can dictate site-specific initiation of DNA replication in Xenopus egg extracts *J. Cell Biol.* **135** 1207–18
[7] Fox C A and Weinreich M 2008 Beyond heterochromatin SIR2 inhibits the initiation of DNA replication *Cell Cycle* **7** 3330–4
[8] Ellis R J 2001 Macromolecular crowding: obvious but underappreciated *Trends Biochem. Sci.* **26** 597–604
[9] Beuthan J, Minet O, Helfmann J, Herrig M and Muller G 1996 The spatial variation of the refractive index in biological cells *Phys. Med. Biol.* **41** 369–82
[10] Perelman L T *et al* 1998 Observation of periodic fine structure in reflectance from biological tissue: a new technique for measuring nuclear size distribution *Phys. Rev. Lett.* **80** 627–30
[11] Mourant J R *et al* 1995 Spectroscopic diagnosis of bladder cancer with elastic light scattering *Lasers Surg. Med.* **17** 350–7
[12] Sokolov K, Drezek R, Gossage K and Richards-Kortum R 1999 Reflectance spectroscopy with polarized light: is it sensitive to cellular and nuclear morphology *Opt. Express* **5** 302–17
[13] Coffey D S 1998 Self-organization, complexity and chaos: the new biology for medicine *Nat. Med.* **4** 882–5
[14] Born M and Wolf E 1999 *Principles Of Optics : Electromagnetic Theory of Propagation, Interference and Diffraction of Light* vol 952 7th edn (Cambridge, New York: Cambridge University Press) pp xxxiii
[15] Subramanian H *et al* 2008 Optical methodology for detecting histologically unapparent nanoscale consequences of genetic alterations in biological cells *Proc. Natl Acad. Sci. USA* **105** 20118–23
[16] Subramanian H *et al* 2009 Partial-wave microscopic spectroscopy detects subwavelength refractive index fluctuations: an application to cancer diagnosis *Opt. Lett.* **34** 518–20
[17] Subramanian H *et al* 2009 Nanoscale cellular changes in field carcinogenesis detected by partial wave spectroscopy *Cancer Res.* **69** 5357–63
[18] Bozzola J J and L D R 1999 *Electron Microscopy* 2nd edn Q4
[19] Leapman R D 1986 Scanning-transmission electron-microscope (stem) elemental mapping by electron energy-loss spectroscopy *Ann. N Y Acad. Sci.* **483** 326–38
[20] Pradhan P and Kumar N 1994 Localization of light in coherently amplifying random-media *Phys. Rev.* B **50** 9644–47
[21] Pradhan P and Sridhar S 2002 From chaos to disorder: statistics of the eigenfunctions of microwave cavities *Pramana-J. Phys.* **58** 333–41
[22] Schwartz T, Bartal G, Fishman S and Segev M 2007 Transport and Anderson localization in disordered two-dimensional photonic lattices *Nature* **446** 52–5
[23] Prigodin V N and Altshuler B L 1998 Long-range spatial correlations of eigenfunctions in quantum disordered systems *Phys. Rev. Lett.* **80** 1944–7
[24] Pradhan P, Damania D, Joshi H, Turzhitsky V, Subramanian H, Roy H K, Taflove A, Dravid V and Backman V 2010 Quantification of nanoscale density fluctuations using electron microscopy: light-localization properties of biological cells *Appl. Phys. Lett.* **97** 243704–6
[25] Zeitler E and Bahr G F 1962 Photometric procedure for weight determination of submicroscopic articles quantitative electron microscopy *J. Appl. Phys.* **33** 847
[26] Loferer-Krossbacher M, Klima J and Psenner R 1998 Determination of bacterial cell dry mass by transmission electron microscopy and densitometric image analysis *Appl. Environ. Microbiol.* **64** 688–94
[27] Barer R, Ross K F A and Tkaczyk S 1953 Refractometry of living cells *Nature* **171** 720–4
[28] Davies H G and Wilkins M H F 1952 Interference microscopy and mass determination *Nature* **169** 541
[29] Lee P A and Ramakrishnan T V 1985 Disordered electronic systems *Rev. Mod. Phys.* **57** 287–337
[30] Schmitt J M and Kumar G 1996 Turbulent nature of refractive-index variations in biological tissue *Opt. Lett.* **21** 1310–2
[31] Bernstein C, Bernstein H, Payne C M, Dvorak K and Garewal H 2008 Field defects in progression to gastrointestinal tract cancers *Cancer Lett.* **260** 1–10
[32] Dakubo G D, Jakupciak J P, Birch-Machin M A and Parr R L 2007 Clinical implications and utility of field cancerization *Cancer Cell Int.* **7** 2
[33] Atkin W S and Saunders B P 2002 Surveillance guidelines after removal of colorectal adenomatous polyps *Gut* **51** V6-9
[34] Butterly L F, Chase M P, Pohl H and Fiarman G S 2006 Prevalence of clinically important histology in small adenomas *Clin. Gastroenterol. Hepatol.* **4** 343–8
[35] van Rijn J C *et al* 2006 Polyp miss rate determined by tandem colonoscopy: a systematic review *Am. J. Gastroenterol.* **101** 343–50
[36] Richter K, Nessling M and Lichter P 2007 Experimental evidence for the influence of molecular crowding on nuclear architecture *J. Cell Sci.* **120** 1673–80
[37] Damania D, Subramanian H, Tiwari A K, Stypula Y, Kunte D, Q5 Pradhan P, Roy H K and Backman V 2010 Role of

cytoskeleton in controlling the disorder strength of cellular nanoscale architecture *Biophys. J.* at press

[38] Kopelovich L, Conlon S and Pollack R 1977 Defective organization of actin in cultured skin fibroblasts from patients with inherited adenocarcinoma *Proc. Natl Acad. Sci. USA* **74** 3019–22

[39] Wax A *et al* 2002 Cellular organization and substructure measured using angle-resolved low-coherence interferometry *Biophys. J.* **82** 2256–64

[40] Wax A *et al* 2005 Prospective grading of neoplastic change in rat esophagus epithelium using angle-resolved low-coherence interferometry *J. Biomed. Opt.***10**